Nanoscale

PAPER

View Article Online
View Journal | View Issue

Check for updates

Cite this: *Nanoscale*, 2024, **16**, 708

Strongly coupled plasmonic metal nanoparticles with reversible pH-responsiveness and highly reproducible SERS in solution†

Zichao Wei, [a] Audrey Vandergriff,[a] Chung-Hao Liu, [b] Maham Liaqat,[a] Mu-Ping Nieh, [b,c,d] Yu Lei[d] and Jie He *[a,b,c]

We report a facile method to prepare polymer-grafted plasmonic metal nanoparticles (NPs) that exhibit pH-responsive surface-enhanced Raman scattering (SERS). The concept is based on the use of pH-responsive polymers, such as poly(acrylic acid) (PAA) and poly(allylamine hydrochloride) (PAH), as multidentate ligands to wrap around the surface of NPs instead of forming polymer brushes. Upon changing the solvent quality, the grafted pH-responsive polymers would drive reversible aggregation of NPs, leading to a decreased interparticle distance. This creates numerous hot spots, resulting in a secondary enhancement of SERS as compared to the SERS from discrete NPs. For negatively charged PAA-grafted NPs, the SERS response at pH 2.5 showed a secondary enhancement of up to 10^4-fold as compared to the response for discrete NPs at pH 12. Similarly, positively charged PAH-grafted AuNPs showed an opposite response to pH. We demonstrated that enhanced SERS with thiol-containing and charged molecular probes was indeed from the pH-driven solubility change of polymer ligands. Our method is different from the conventional SERS sensors in the solid state. With pH-responsive polymer-grafted NPs, SERS can be performed in solution with high reproducibility and sensitivity but without the need for sample pre-concentration. These findings could pave the way for innovative designs of polymer ligands for metal NPs where polymer ligands do not compromise interparticle plasmon coupling.

Received 9th October 2023,
Accepted 22nd November 2023

DOI: 10.1039/d3nr05071h

rsc.li/nanoscale

Open Access Article. Published on 22 2023. Downloaded on 2025/11/21 6:03:50.
This article is licensed under a Creative Commons Attribution 3.0 Unported Licence.

Introduction

Plasmonic metal nanoparticles (NPs) exhibit a unique localized surface plasmonic resonance (LSPR), arising from the collective oscillation of free electrons on their surfaces resonating with electromagnetic waves at specific wavelengths.[1,2] Based on the LSPR of plasmonic NPs, there has been tremendous interest in their use for chemical and biological sensing, *e.g.*, surface-enhanced Raman scattering (SERS). SERS can amplify the Raman signal of organic molecules adsorbed onto metal NPs, due to the enhanced resonance of the local electric field intensity associated with plasmonic metal materials or NPs, *e.g.*, silver NPs (AgNPs) and gold NPs (AuNPs).[1,3–10] Consequently, SERS stands as a potent tool with high sensitivity to detect target molecules at low concentrations.[5,11–13]

During SERS-enabled detection when an incoming electromagnetic wave resonates with the coherent oscillation of free electrons, it generates an enhanced electric near field commonly referred to as 'hot spots'. These hot spots have the potential to substantially amplify signals, often providing an enhancement factor in the range of 10^4 to 10^7.[14] Controlled synthesis[15,16] and self-assembly of metal NPs[17–19] can effectively create hot spots with a higher plasmonic field, as compared to the thin films and/or spherical NPs. This can be achieved through methods such as designing NPs with sharp edge or tip sites that produce a more intense local field and reducing the interparticle distance between NPs with strong plasmon coupling. The interparticle plasmon coupling could occur when NPs are in close proximity, typically within a range of about 2.5 times their size. This proximity-induced interparticle coupling leads to the overlap of the two plasmon fields along with a noticeable red shift in the average plasmon resonance peak wavelength ($\Delta\lambda_{LSPR}$). The coupling strength, however, shows an exponential decay with the interparticle distance. For example, in the case of spherical AuNPs, $\Delta\lambda_{LSPR}$ decays exponentially as $\Delta\lambda_{LSPR} \propto e^{-l}$,[20–22] where l is the interparticle distance. When the interparticle distance increases, the near-field plasmon coupling is diminished, leading to minimal SERS enhancement. Therefore, how to control the interparticle assemblies of

[a]*Department of Chemistry, University of Connecticut, 55 N. Eagleville Road, Unit 3060, Storrs, Connecticut 06269-3060, USA. E-mail: jie.he@uconn.edu*
[b]*Polymer Program, University of Connecticut, Storrs, CT 06269, USA*
[c]*Institute of Materials Science, University of Connecticut, Storrs, CT 06269, USA*
[d]*Department of Chemical and Biomolecular Engineering, University of Connecticut, Storrs, CT 06269, USA*

† Electronic supplementary information (ESI) available. See DOI: https://doi.org/10.1039/d3nr05071h

This journal is © The Royal Society of Chemistry 2024

Open Access Article. Published on 22 2023. Downloaded on 2025/11/21 6:03:50.
This article is licensed under a Creative Commons Attribution 3.0 Unported Licence.

metal NPs as a means to enhance the SERS signal of molecular probes has been a key to improving the sensitivity in SERS detection.[23,24]

In the wet-chemical approach, the interparticle distance of metal NPs is usually determined by their surface ligands. These ligands are organic molecules or polymers that cap the surface of metal NPs.[25–28] An obvious example is the use of DNA as a spacer to vary the interparticle distance as demonstrated by Reinhard *et al.*[22] The DNA "soft shell" could accurately control the assembly process *via* the biotin and digoxigenin interaction to change the particle distance by the number of base pairs. With molecular ligands despite ill-defined clustered NPs, those ligand-modified NPs can aggregate when driven by external stimuli, such as pH, temperature, and hydrophobic force, leading to the formation of NP clusters that give rise to interparticle plasmon coupling.[29–33] However, for larger plasmonic NPs, those molecular ligands are too short to balance the strong interparticle attraction and, therefore, offer poor colloidal stability in solution. Conversely, polymer-grafted plasmonic metal nanoparticles (PGNPs) are composed of polymer ligands grafted on metal NP cores.[26,34,35] Polymer ligands with high steric hindrance provide remarkable colloidal stability to metal NPs. Upon changing the solvent quality to the polymer, PGNPs can cluster, allowing the precise control of the nanogap between adjacent metal NPs.[36–40] Differences in chain lengths and the grafting density are two important characteristics to control the interparticle distance, and, consequently, manipulate plasmonic coupling. The typical polymer ligands, such as thiol-tethered polymers, can bind with metal NPs but with an extended brush-like conformation. Such brush-like polymer chains, even in their poor solvents, create a large interparticle distance for the plasmon coupling of metal NPs.[41–43] Therefore, the SERS enhancement provided by PGNPs is usually on par with that of individual NPs.[44–46] To achieve a shorter interparticle distance and a stronger interparticle plasmonic coupling, the manner in which polymer ligands bind to the surface of metal NPs is crucial.

We herein report a facile method to prepare pH-responsive PGNPs where polymers can attach the surface of metal NPs to allow reversible aggregation and dispersion of the metal NPs in response to pH change. Our method is simply based on the use of pH-responsive polymers, *e.g.* poly(acrylic acid) (PAA)[47,48] or poly(allylamine hydrochloride) (PAH),[49] through the "grafting-to" and *in situ* growth method, respectively. PAA and PAH have multiple weak binding motifs, *e.g.*, COOH and NH_2, respectively, where polymer chains with maximized binding would wrap the surface of metal NPs. When the pH is altered to trigger the solubility change of polymer ligands, strong plasmon coupling was evidenced from the dramatic color change and the LSPR shift in the UV-vis spectra. The NP aggregates exhibited a reduced interparticle distance to create hot spots for the "second" SERS enhancement of additional 10^3–10^4 fold, as compared to the SERS observed on discrete NPs (Scheme 1). With those charged polymer ligands, two types of SERS probes have been examined: thiol-containing and/or charged molecules. One of the advantages is that SERS detection could be done in water with high reproducibility and reversibility. There is no need for additional purification or pre-concentration steps for sample analysis. The analysis does not require any time-consumable synthesis, and all materials used in this study, including polymers, are readily available at low cost. The SERS enhancement could be turned ON and OFF by switching the pH to vary the hydrophobicity of polymers. The versatility of our method enables the detection of a broad range of substrates including glucose and pesticides, directly from solution measurement.

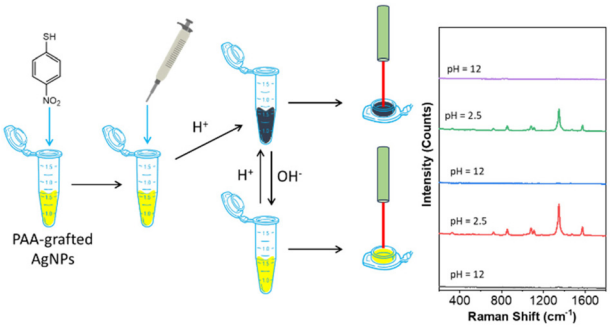

Scheme 1 A flow chart showing pH-responsive SERS detection with PAA-grafted AgNPs.

Results and discussion

pH-responsive PGNPs

PAA-modified NPs were prepared through a one-phase ligand exchange in water. Typically for AgNPs, 40 mL of citrate-capped AgNPs (0.1 mg mL^{-1}, 27 nm) was first centrifuged and about 100 μL of the concentrated solution was collected.[50] 5 mg of PAA (MW: 1200 g mol^{-1}) was dissolved in 20 mL of deionized water. Then, the concentrated solution of AgNPs was added dropwise to the PAA aqueous solution under vigorous sonication. The mixture was incubated for 24 h at room temperature. The free PAA was removed by centrifuging three times. PAA has a pK_a of 4.5.[51] The pH-responsiveness was examined by titrating with 50 mM H_3PO_4 (note that HCl reacts with AgNPs). As given in Fig. 1a, PAA-grafted AgNPs have a yellow color at natural pH, and it changed to a greenish black color at pH 2.5 (Fig. 1a). The LSPR peak of AgNPs had a redshift from 414 nm to 673 nm, suggesting the aggregation of PAA-grafted AgNPs upon the addition of acid. The acid can trigger the aggregation of PAA-grafted AgNPs because the re-protonation of PAA makes it less soluble in water. This aggregation is completely reversible. It could be disassembled by titrating with 0.05 M of NaOH solution. Fig. 1a shows the recovery of the yellow solution color at pH 12. From UV-vis, the LSPR peak recovered to 414 nm with decreased absorbance due to dilution (Fig. 1d). This change was further revealed by transmission electron microscopy (TEM). Fig. 1c shows the representative TEM image of PAA-grafted AgNPs at pH 12. AgNPs were well-dispersed under basic conditions because the nega-

Open Access Article. Published on 22 2023. Downloaded on 2025/11/21 6:03:50.
This article is licensed under a Creative Commons Attribution 3.0 Unported Licence.

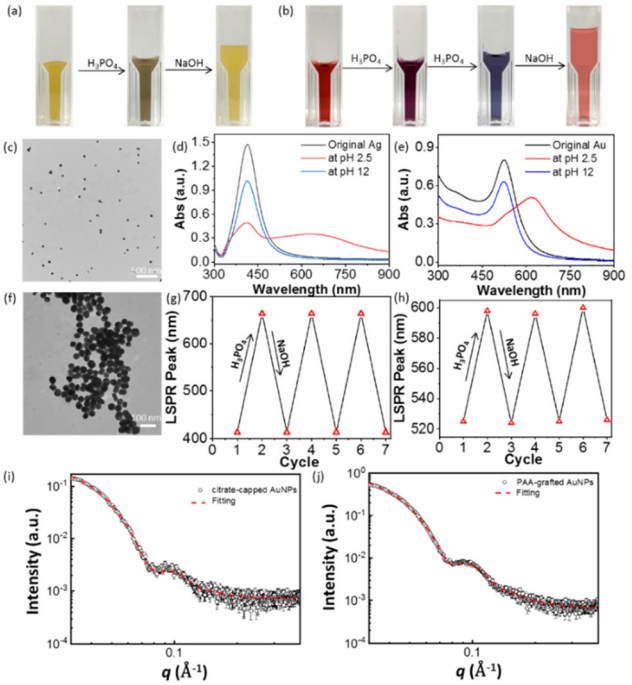

Fig. 1 (a and b) pH-responsiveness of (a) PAA-grafted AgNPs (0.2 mg mL^{-1} of AgNPs) and (b) PAA-grafted AuNPs. The color change was triggered by adding 0.5 M phosphate acid (H_3PO_4) and sodium hydroxide (NaOH) to tune the solution pH. (c and f) TEM images showing morphologies of PAA-AgNPs at pH values of (c) 2.5 and (f) 12. (d) UV-vis spectra showing the LSPR change of PAA-grafted AgNPs and (e) PAA-grafted AuNPs at different pH values. (g and h) Reversibility of the LSPR shift of (g) PAA-grafted AgNPs and (h) PAA-grafted AuNPs upon titration with H_3PO_4 and NaOH alternatively. (i and j) SAXS patterns of AuNPs: citrate-capped AuNPs (i) and PAA-grafted AuNPs (j) measured in water.

tively charged PAA on the surface of AgNPs is water-soluble and provides strong electrostatic repulsion to prevent the aggregation of AgNPs. At pH 2.5, PAA-grafted AgNPs aggregated under acidic conditions since the re-protonation of PAA is not water-soluble and triggers the disordered assembly of AgNPs (Fig. 1f). The assembly and disassembly of AgNPs are completely reversible to the pH change. Fig. 1g shows the reversibility switch of the LSPR peak by alternatively adding 20 μL of 0.05 M H_3PO_4 solution and 0.05 M NaOH solution to the aqueous solution of PAA-grafted AgNPs. The corresponding LSPR shifted between 414 nm and 673 nm with a decrease in absorbance during each cycle. Those results confirm that PAA can tune the assembly and disassembly with good reversibility and reproducibility. Note that, without PAA, the aggregation caused by an acid or base is irreversible.

This method is applicable to AuNPs as well. After similar surface modification with citrate-capped AuNPs (12 nm), PAA-grafted AuNPs (0.2 mg mL^{-1}) are colloidally stable with an LSPR of 524 nm (Fig. 1h). Fig. 1b shows the color switch from red gradually to purple and then to blue with the addition of H_3PO_4 solution. From the UV-vis spectra, the LSPR peak of PAA-grafted AuNPs changed from 524 nm to 611 nm at pH 2.5. Similarly, the increase of acidity can lower the solubility of PAA to trigger the aggregation of AuNPs. The red color of discrete AuNPs could be recovered by adding NaOH (Fig. 1b), along with the shift of the corresponding LSPR peak to 524 nm (Fig. 1e). Likewise, the reversibility and reproducibility are similar to that of PAA-grafted AgNPs (Fig. 1h).

To get more insights into the reversible and strong LSPR coupling of PAA-grafted AuNPs, small-angle X-ray scattering (SAXS) was used to estimate the shell thickness of polymer ligands. The scattering profiles are given in Fig. 1i and j. A core–shell spherical model (CSS) was applied to citrate-capped and PAA-grafted AuNPs. The shell thickness in the case of PAA-AuNPs is <10 (±1) Å, suggesting that the COOH groups closely adhere to AuNPs and the PAA chains wrap the surface of AuNPs instead of forming extended polymer brushes in PGNPs. While PAA-grafted NPs show a fully reversible color switch under an acid and base, PAA as ligands should have a surface coverage on NPs to avoid irreversible aggregation. For PGNPs, there have been a few reports on charged polymers, *e.g.* copolymers of PAA as ligands for plasmonic NPs.[52–56] For example, the copolymers of poly(styrene-*co*-acrylic acid) could show strong plasmon coupling similar to that of PAA.[52] It is very likely that multiple carboxyl acid groups would change the confirmation of polymers bound with NPs.

Likewise, the pH-responsiveness of PGNPs can be applied to PAH that has opposite responsiveness to an acid/base, *i.e.*, dispersed in an acid and aggregated in a base. Therefore, we prepared AuNPs with PAH through a thermal reduction method with PAH as a reducing agent under reflex conditions.[49] The as-synthesized PAH-grafted AuNPs were purified by centrifuging the solution three times and redispersed in DI water. The TEM image in Fig. 2b reveals the average size of

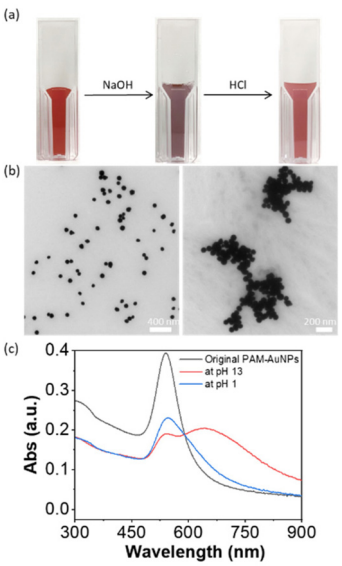

Fig. 2 (a) Pictures showing the pH-responsive properties of PAH-grafted AuNPs with 0.5 M NaOH solution and 1 M HCl solution. (b) TEM images showing the morphologies of PAH-AuNPs at pH values of 1 (left) and 13 (right). (c) UV-vis spectra showing the LSPR peak of PAH-AuNPs, and the corresponding LSPR peaks at pH values of 1 and 13.

This journal is © The Royal Society of Chemistry 2024

Open Access Article. Published on 22 2023. Downloaded on 2025/11/21 6:03:50.
This article is licensed under a Creative Commons Attribution 3.0 Unported Licence.

AuNPs, around 37 nm. PAH-grafted AuNPs show a single LSPR peak at 540 nm.

The pH-responsiveness of PAH-grafted AuNPs was examined similarly. Upon titrating with NaOH solution to pH 13, the solution color changed from deep red to purple. From UV-vis spectroscopy, a new LSPR peak was observed at 648 nm. This indicates that the addition of a base could induce the aggregation of PAH-grafted AuNPs. Upon adjusting the pH to 1 by adding 1 M HCl solution, the color changed to red. The LSPR peaks at longer wavelengths disappeared and a single LSPR peak was observed at 543 nm with a decreased intensity due to dilution. However, there was a notable tail on the LSPR peak of disassembled AuNPs, presumably due to the high binding strength of amines to AuNPs. The pH-responsive aggregation was monitored by TEM. As shown in Fig. 2b, the PAH-AuNPs were well distributed at pH 13 while more dispersed AuNPs were seen at pH 1. This suggests that the solubility of charged PAH on the surface of AuNPs could also reversibly shift the plasmon coupling of AuNPs, similar to that of PAA but in an opposite fashion.

SERS of molecular thiolates

SERS uses the inelastic light scattering of molecules absorbed on plasmonic NPs. To get better sensitivity, creating a nanogap as a "hot spot" can enhance the local field strength to improve sensitivity. The typical interparticle distance in polymer-grafted NP assemblies is in the range of 5–20 nm. The SERS enhancement factor, therefore, is usually low. For example, in the case of gold nanorods (AuNRs), the end-to-end self-assembly guided by hydrophobic polystyrene (PS) can enhance the Raman signal of oxazine; but, the SERS enhancement factor is only about 2–3 fold, as compared to individual AuNRs.[44] With molecular ligands, the SERS enhancement factor could increase to two orders of magnitude in the clusters of spherical AuNPs.[18]

In both cases of PAA and PAH, we have observed strong plasmon coupling with a change in pH. We therefore further examined how the formation of the hot spot upon disorder aggregation would improve their SERS enhancement in solution. Taking PAA-grafted AgNPs as an example, we used 4-nitrothiophenol (4-NTP, Fig. 3a) as a Raman reporter to chemically bond to AgNPs through metal-thiolate.[57,58] In PAA-grafted AgNPs under natural conditions, we first added 4-NTP at a concentration of 1 μM and the solution was incubated for 5 min before any measurement. The SERS measurements were done in solution with a starting volume of 130 μL in a testing tube by titrating with 0.5 M H_3PO_4 and 0.5 M NaOH. At pH 2, the typical SERS vibration peaks of 4-NTP can be identified. The Raman peaks at 1100, 1343 and 1571 cm^{-1} correspond to the C–H bending, the symmetric stretching of NO_2 and the C–C stretching of the phenyl ring. In contrast, when the pH increased to 12, no 4-NTP SERS vibration bands were observed.

The results strongly suggested that the assembled PAA-grafted AgNPs would significantly enhance the SERS response due to the formation of interparticle hot spots, while the well-dispersed PAA-grafted AgNPs under basic conditions did not

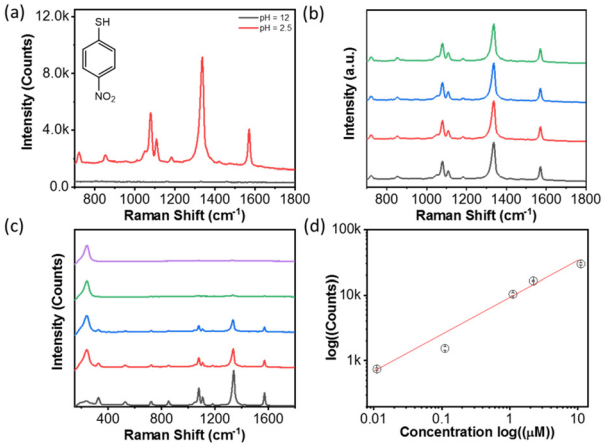

Fig. 3 (a) SERS response of 4-NTP at a concentration of 1 μM on PAA-grafted AgNPs at pH 2.5 and 12. (b) SERS spectra of 4-NTP with PAA-AgNPs assemblies at a pH value of 2.5 at different testing sites. (c) SERS response of PAA-AgNPs for 4-NTP at a concentration range of 0.01–10 μM. (d) The plot showing the intensity changes of the strongest peak at 1343 cm^{-1} at different pH values by continuously adding 0.5 mM H_3PO_4 solution.

strongly enhance the SERS signal due to the lack of interparticle plasmon coupling. Fig. 3b shows the highly reproducible spectra at different locations of the solution. Given the solution uniformity and homogeneity, the solution SERS is more reproducible than the conventional SERS performed on a solid substrate. It should be noted that SERS measurements were carried out without any sample pre-purification or pre-concentration. Meanwhile, we examine the SERS signal at different positions in solution. All spectra have similar peak intensities, and the average count is $(8.1 \pm 0.2) \times 10^3$ at 1343 cm^{-1}. Therefore, pH-triggered aggregation would enhance the SERS response at least by 8000 fold for 4-NTP.

To examine the SERS sensitivity of PAA-grafted AgNPs, the different concentrations of 4-NTP were examined. The final substrate concentration ranges from 10 μM to 10 nM, while 20 μL of 0.5 M H_3PO_4 solution was added to trigger the assembly of AgNPs. Fig. 3c shows the Raman spectra of 4-NTP at various concentrations. The plot in Fig. 3d is the logarithm concentration against the peak intensity at 1343 cm^{-1}. The linear relationship is seen, and the detection limit is down to 10 nM without optimizing the concentration of AgNPs. The calculated detection limit of 4-nitrothiophenol using PAA-Ag is 3.3×10^{-7} M, close to that on gold and silver-based SERS sensors in solid films or on chips usually in the range of 10^{-8}–10^{-9} M.[59,60] One of the advantages in solution is that SERS detection could be done in water with high reproducibility and reversibility. No additional purification or pre-concentration steps are needed for sample analysis, different from the solid state. The relatively broad concentration range suggests that there is great potential to use PAA-grafted AgNPs in SERS sensors in solution.

To confirm whether the enhancement is from the solubility of polymers, the SERS intensity of 4-NTP against pH was

Open Access Article. Published on 22 2023. Downloaded on 2025/11/21 6:03:50.
This article is licensed under a Creative Commons Attribution 3.0 Unported Licence.

examined during acid titration while fixing the concentration of 4-NTP at 1 μM. Fig. 4a plots the SERS spectra of 4-NTP in the course of decreasing the pH to 2.5. There was a clear increase of the peak intensity by lowering the pH. The maximum peak intensity at 1343 cm^{-1} was plotted against the pH of the solution as displayed in Fig. 4b. An abrupt intensity transition was seen at pH ~4, close to the pK_a of PAA. The results are strongly indicative of the SERS enhancement from PAA-guided NP aggregation. In other words, lowering the pH resulted in the formation of hot spots by changing the solubility of the PAA that wraps the surface of AgNPs. We should note that the slow titration of the acid would give a slightly lower SERS enhancement, likely due to the formation of small aggregates at a slower kinetics. Nevertheless, the second SERS enhancement triggered by pH is obvious as shown in Fig. 4b. Furthermore, the SERS response shows the reversibility at different pH values. By adding 0.5 M NaOH solution to pH 12, the SERS response of 4-NTP was minimum (Fig. 4c). With reverse titration of 0.5 M H_3PO_4, the typical vibration bands of 4-NTP appeared. This process was highly reversible by changing the pH several times, although the decreased peak intensity was seen (Fig. 4d). All results suggested that the SERS enhancement based on pH-triggered reversible aggregation could be switched between ON/OFF on demand for sensing applications.

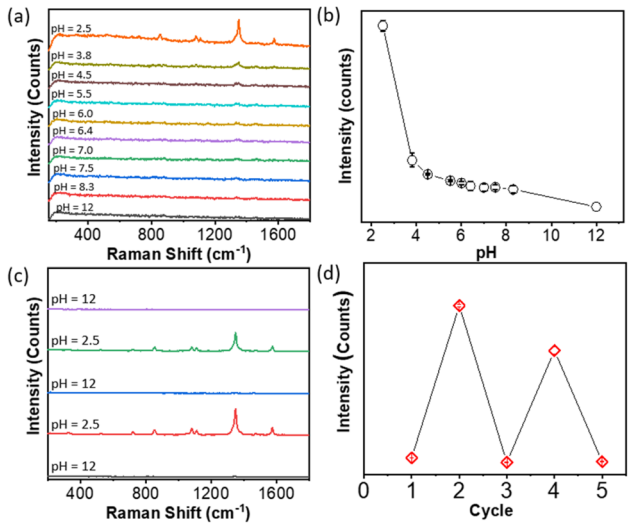

Fig. 4 (a) SERS response of PAA-grafted AgNPs for 4-NTP at 0.5 μM at different pH values of 2.5–12. (b) Plotting the peak intensity at 1343 cm^{-1} against the solution pH by titrating 0.5 mM H_3PO_4. (c) Raman spectra showing the pH-responsive SERS of 4-NTP with PAA-grafted AgNPs at pH values of 2.5 and 12, respectively. (d) Plotting the peak intensity of 4-NTP at 1343 cm^{-1} at alternative pH values of 2.5 and 12.

We further examined five typical Raman reporters, *e.g.*, 4-aminothiophenol, 4-mercaptopyridine, thiophenol, 4-mercaptophenylboronic acid (4-MCBA) and 4-mercaptobenzoic acid (4-MCTA), to investigate the generality of our approach. The results are summarized in Table 1. All reported counts were carried out with reporters at a concentration of 1 μM. The maximum peak intensities in the spectra were used to determine the pH-driven SERS enhancement at pH 2.5. In all cases, there is no SERS response measurable at pH 12. By lowering the pH to 2.5, typical Raman vibration bands can be found with the SERS response (Fig. S1–S5†). The enhancement was 3–4 orders of magnitude as compared to discrete AgNPs at pH 12. The broad substrate ranges can be applied to a powerful SERS sensor for thiol-containing phenyl molecules. In addition, a similar SERS response has been observed for PAA-grafted AuNPs and PAH-grafted AuNPs (Fig. 5). At the same time, the solution-based enhancement is facile, fast and highly reproducible throughout the solution, potentially offering a complementary measurement of SERS in the solid state.

PAH-modified NPs can also be applied to enhance SERS while the pH-response of SERS enhancement is opposite to that of PAA-modified NPs. Using PAH-grafted AuNPs as an example, 4-MCTA was first bound with AuNPs *via* the metal–ligand interaction (Fig. 5a). The concentration of 4-MCTA was kept at 10 μM. By adding HCl to lower the pH to 2.5, a weak SERS spectrum of 4-MCTA was seen. The peaks at 1074 cm^{-1} and 1585 cm^{-1} are assigned to the C–H bending and the C–C stretching of the aromatic ring. The peak intensity at 1074 cm^{-1} is 130 counts. After adding NaOH to pH 12 the mixture with the same concentration of 4-MCTA showed a much enhanced SERS response. The spectral intensity at 1074 cm^{-1} increases to 5.8×10^3 counts, about 45-fold compared to the same sample under acidic conditions.

Table 1 Summarization of the SERS intensity of different thiol-containing reporters

Reporter	pH	Concentration (μM)	Raman shift (cm^{-1})	Intensity (counts)
4-Aminothiophenol	12	1.0	1078	0
	2.5	1.0	1078	2.7×10^4
4-Mercaptopyridine	12	1.0	1003	0
	2.5	1.0	1003	4.9×10^4
Thiolphenol	12	1.0	1070	0
	2.5	1.0	1070	3.4×10^3
4-Mercaptophenylboronic acid	12	1.0	1070	0
	2.5	1.0	1070	2.2×10^3
4-Mercaptobenzoic acid	12	1.0	1076	0
	2.5	1.0	1076	3.1×10^3

This journal is © The Royal Society of Chemistry 2024

Open Access Article. Published on 22 2023. Downloaded on 2025/11/21 6:03:50.
This article is licensed under a Creative Commons Attribution 3.0 Unported Licence.

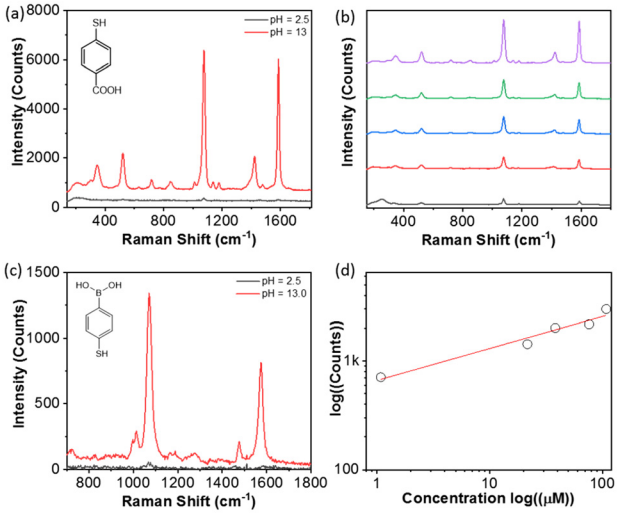

Fig. 5 (a) SERS response of PAH-grafted AuNPs for 4-MCTA at pH values of 1 and 13. (b) SERS response of 4-MCTA at a concentration range of 1–100 μM with PAH-grafted AuNPs. (c) SERS response of 4-MCBA at pH values of 1 and 13 with PAH-grafted AuNPs. (d) Plotting the peak intensity at 1074 cm^{-1} at a pH value of 13 against the concentration of 4-MCBA.

Meanwhile, a similar substrate, such as 4-MCBA, shows an identical response to pH where much enhanced SERS signals were observed under basic conditions.

SERS of charged reporters

PAA-grafted metal NPs are negatively charged; therefore, they can bind with positively charged Raman reporters as well.[61,62] The electrostatic interaction between PAA and charged substrates provides alternative ways to board the target molecules. We chose rhodamine 6G (R6G, Fig. 6a) as a model compound because it is a positively charged conjugated compound with a strong absorbance at 621 nm that resonates with AgNP aggregates. For SERS measurement, the solution of R6G was first added into 130 μL of PAA-AgNPs for 5 min. Then, 0.5 M H_3PO_4 solution was added to the solution to trigger the aggregation of AgNPs with gentle shaking for 1 min. Fig. 5a shows the SERS spectrum of R6G measured at pH 2.5. The typical vibration bands of R6G can be observed at 1511, 1362 and 1310 cm^{-1}, assigned to the C–C stretching in aromatic rings and alkyl groups (Fig. 6a). The peaks at 1182 and 1125 cm^{-1} are assigned to the C–H in-plane bending and the peaks at 610 and 770 cm^{-1} are assigned to C–C–C ring in-plane bending and C–H out of plane bending, respectively. With the increase of pH by adding 0.5 M NaOH, there are no vibration bands under basic conditions (Fig. 6a). Those results suggested that PAA-grafted AgNPs could adsorb R6G through electrostatic interactions and enhance its SERS signal. In the absence of thiol in R6G, it was not chemically bound with AgNPs while the negatively charged PAA could physically adsorb R6G to allow SERS measurement. All tests were carried out four times (Fig. 6b). AgNP aggregates with R6G presented good reproducibility. The SERS spectra of R6G at different concentrations in the range of 3.6 nM to 3.6 μM were collected at pH 2.5 (Fig. 6c). Similarly, the peak intensity of R6G increases with the concentration of R6G. Fig. 5d shows the plot of the concentration against the peak intensity at 1511 cm^{-1} in logarithm. A linear relationship was seen with the minimum detectable concentration down to 3.6 nM.

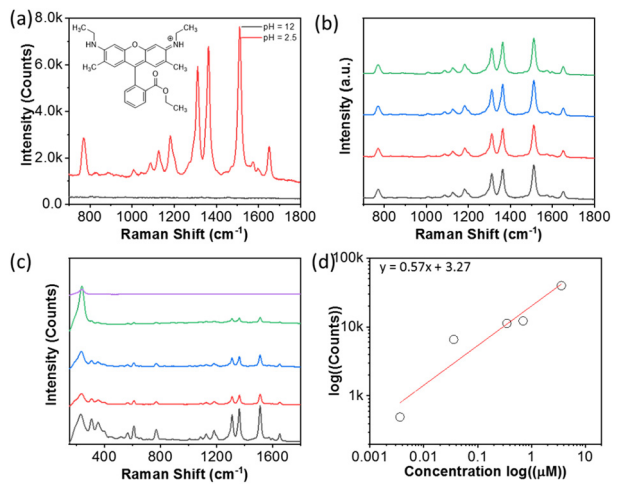

Fig. 6 (a) SERS response of PAA-grafted AgNPs for R6G at 0.36 μM. (b) SERS spectra of R6G PAA-grafted AgNPs at pH 2.5 for different solution spots. (c) SERS response of R6G in the concentration range of 3.6 nM–3.6 μM with PAA-grafted AgNPs. (d) Plotting the peak intensity at 1341 cm^{-1} against the concentration of R6G.

The SERS response of R6G to pH has a similar trend to 4-NTP. Fig. 7a shows the titration of PAA-grafted AgNPs and R6G with H_3PO_4 from pH 12 to 2.5. No peak of R6G was seen in the pH range of 12 to 7, because AgNPs were well-dispersed in water. The peaks of R6G appeared when the pH reached 6.5 and the peak intensity gradually increased with a further decrease in pH (Fig. 7b). Similarly, the SERS enhancement was slightly smaller during titration as a result of kinetics-limited clustering of AgNPs. The reversibility of pH-responsiveness was confirmed by alternatively changing the pH value between 12 and 2.5 (Fig. 7c and d). The R6G vibrational peaks were pronounced at pH 2.5 and all the peaks were minimum at pH 12.

We also examined the variability of charged substrates (Table 2). Three Raman reporters including crystal violet, methylene blue and Nile Blue (Fig. S6–S8†) were chosen as positively charged substrates to bind with PAA electrostatically. All substrates were studied at a concentration of 0.4 μM. At pH 12, no peaks were observed (Table 2), similar to that of R6G under the same basic conditions. In contrast, typical vibration bands were clear by adding H_3PO_4 to pH 2.5. For the crystal violet (Fig. S6†), the spectra show the main vibration peaks at 1620 cm^{-1} for the C–C stretching of aromatic rings, 1372 cm^{-1} for C–N stretching of the phenyl ring, 1175 cm^{-1} for in-plane aromatic C–H bending, and 803 cm^{-1} for out of plane C–H bending, respectively. For methylene blue (Fig. S7†), the typical peaks at 1618 cm^{-1} and 1500 cm^{-1} for the C–C stretching of aromatic rings, 1397 cm^{-1} for symmetrical stretching of C–N, 1181 cm^{-1} for stretching of C–N, and 777 cm^{-1} for

Open Access Article. Published on 22 2023. Downloaded on 2025/11/21 6:03:50.
This article is licensed under a Creative Commons Attribution 3.0 Unported Licence.

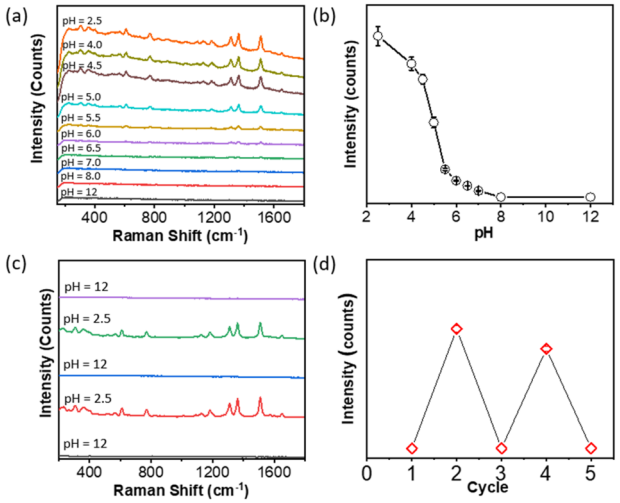

Fig. 7 (a) SERS response of PAA-AgNPs for R6G at a concentration of 1 μM at different pH values of ~2.5–12. (b) The plot showing the intensity changes of the strongest vibration peak at 1509 cm^{-1} at different pH values by continuously adding 0.5 mM H_3PO_4 solution. (c) Raman spectra showing the pH responsive SERS of R6G with PAA-AgNPs at pH values of 2.5 and 12, respectively. (d) The plot showing the strongest vibration peak intensity of R6G at 1509 cm^{-1} at pH values of 2.5 and 12.

Table 2 Summarization of the SERS intensities of positively charged molecules

Reporter	pH	Concentration (μM)	Wavelength (nm)	Intensity (counts)
Crystal violet	12	0.4	1621	0
	2.5	0.4	1621	1.5×10^4
Methylene blue	12	0.4	1618	0
	2.5	0.4	1618	7.7×10^3
Rhodamine 6G	12	0.4	1512	0
	2.5	0.4	1512	5.8×10^3
Nile blue	12	0.3	592	0
	2.5	0.3	592	5.3×10^4

stretching of in-plane bending, respectively. For Nile Blue (Fig. S8†), the Raman spectra exhibited prominent peaks at 590 and 661 cm^{-1}, corresponding to the deformations of C–C–C and C–N–C bonds, as well as the in-plane deformation of C–C–C bonds. Those SERS spectra suggest that the positively charged substrates with the electrostatic interaction with PAA can be detected through the SERS enhancement of AgNP aggregates. Therefore, the positively charged substrates could be trapped at the interparticle hot spots to develop their Raman detection method.

Enhanced SERS to detect glucose and pesticides

To explore more practical SERS applications, we have carried out both qualitative and quantitative analyses of glucose and pesticides. It is meaningful to design glucose detection in solution given the application of glucose sensing in blood samples. For glucose detection, PAA-grafted AgNPs were first modified with 4-MCBA at a concentration of 1.0 μM. Glucose

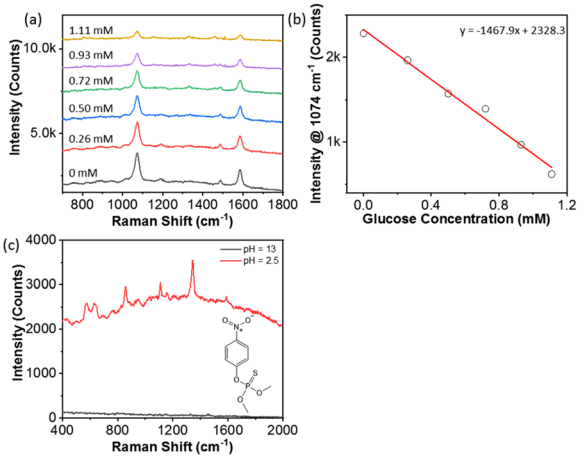

Fig. 8 (a) Glucose detection using 4-MCBA with PAA-grafted AgNPs at concentrations of 0 mM to 1.11 mM of glucose in addition to 0.5 M H_3PO_4 solution. (b) Plotting the peak intensity of 4-MCBA at 1074 cm^{-1} *vs.* glucose concentrations of 0 mM to 1.11 mM. (c) Detection of methyl parathion using PAA-grafted AgNPs at a concentration of 17 ppm after adding H_3PO_4.

couples rapidly with boronic acid where the hydroxyl groups of glucose can form boronate covalently. In SERS spectra, the vibration intensities of 4-MCBA at 1074 and 1586 cm^{-1} would decrease after adding glucose. In our experiments, we added glucose to the above mixture solution of PAA-grafted AgNPs and 4-MCBA. The concentration of glucose was varied from 0 mM to 1.11 mM, slightly below the glucose concertation in blood to test the sensitivity. The corresponding SERS spectra were collected by adding H_3PO_4. In Fig. 8a, the peak intensity at 1074 and 1586 cm^{-1} decreased by increasing the concentration of glucose. This suggested the reaction between the boronic acid and hydroxyl groups of glucose. The corresponding plot of the glucose concentration *vs.* the peak intensity at 1074 cm^{-1} is given in Fig. 8b. A linear relationship with the glucose concentration was observed. This indicated that pH-driven aggregation can be used to quantitatively detect glucose, which is a promising technique for medical sensors.

We examined another application for pesticide detection. Methyl parathion is an extremely hazardous pesticide. Using PAA-grafted AgNPs, we recorded the SERS of methyl parathion at a relatively low concentration of 17 ppm. Methyl parathion is slightly zwitterionic and carries a few O atoms to bind with PAA through either electrostatic or hydrogen bonding. At 17 ppm in solution, PAA-grafted AgNPs were not able to detect methyl parathion at pH 12 as discrete AgNPs. After decreasing the pH to 2.5, the typical vibration peaks of methyl-parathion were observed (Fig. 8c).

Conclusions

In summary, we demonstrated a general and facile method to prepare PGNPs that exhibit pH-responsive Raman enhancement. The concept simply relies on the conformation of

This journal is © The Royal Society of Chemistry 2024

Open Access Article. Published on 22 2023. Downloaded on 2025/11/21 6:03:50.
This article is licensed under a Creative Commons Attribution 3.0 Unported Licence.

polymer ligands on plasmonic NPs. pH-responsive polymers, like PAA and PAH, serve as multidentate ligands with more binding sites wrapped around the surface of NPs. The presence of PAA and PAH endowed pH-responsiveness to AgNPs and AuNPs. At pH 2.5, PAA-grafted NPs aggregated, exhibiting a strong plasmon coupling process that is fully reversible by adjusting the pH to 13. Meanwhile, the aggregates resulted in a smaller interparticle distance, providing numerous hot spots for the secondary enhancement of SERS. When PAA-grafted NPs were tested with thiolate and positively charged SERS probes under basic and acidic conditions, its SERS response at pH 2.5 showed a second enhancement of up to 10^4-fold as compared to the SERS response for discrete NPs at pH 12. The pH titration and the reversible experiments confirmed that this enhancement was derived from the surface ligands of PAA. It is different from the conventional SERS sensors in the solid state, where the SERS of PAA-grafted NPs could be performed in solution with high reproducibility and sensitivity. Similarly, positively charged PAH-grafted AuNPs showed an opposite response to pH. PAA-grafted AgNPs have been demonstrated for sensing glucose and pesticides in solution with reasonable sensitivity. This method we outline here could be a powerful tool for the design of polymer ligands for PGNPs where polymer ligands do not compromise interparticle plasmon coupling.

Experimental

Chemicals and materials

All chemicals were purchased from Aldrich unless others noted. PAA has a molecular weight of 1.2 kg mol^{-1}, and PAH has a molecular weight of 17.5 kg mol^{-1}. Sodium citrate tribasic dihydrate (>99.0%) and silver nitrate ($AgNO_3$) (>98.0%) were purchased from Alfa-Aesar. The ultra-pure water was distilled with a High-Q distillation system (model # 103S).

Synthesis of AgNPs

AgNPs were synthesized using a modified method of previously reported literature.[63] 47.5 mL of deionized water was added in a 250 mL Erlenmeyer flask in a preheated water bath at 100 °C. Subsequently, 50 μL of ascorbic acid solution was injected into boiled deionized water. 2.5 mg of $AgNO_3$ in 25 μL of water was mixed with 1 mL of sodium citrate solution (1 wt%). This solution was incubated for 5 min. It was quickly injected into the solution containing ascorbic acid. The reaction solution changed from colorless to yellow slowly. The reaction mixture was further boiled and stirred for an additional hour. The average size of AgNPs was 27 nm.

Synthesis of AuNPs

Citrated acid capped AuNPs were synthesized according to the previously referenced literature.[38] 100 mg of $HAuCl_4$ was dissolved in 1 L of DI water, and the solution was placed in a preheated water bath at 100 °C. 30 mL of 1 wt% of sodium citrate solution was quickly injected into the $HAuCl_4$ solution and the mixture was stirred for 30 min. AuNPs were collected by centrifuging at 11 000 rpm for 20 min. The average size of AuNPs was about 12 nm confirmed by TEM.

Synthesis of PAH-AuNPs

PAH-grafted AuNPs were synthesized using a modified method from previous literature.[49] Typically, 9 mL of DI water was added to a 20 mL glass vial. 500 μL of 8 mg mL^{-1} $HAuCl_4$ solution and 500 μL of 40 mg mL^{-1} PAH solution were injected into the same vial with vigorous stirring for 30 min. The solution was placed in a boiling water bath and the pale-yellow solution changed to red after 20 min. The solution was stirred for another 1 h. The solution was cooled down to room temperature and free PAH was removed by centrifuging three times. The purified PAH-AuNPs were redispersed to water for further use.

Surface modification of AuNPs/AgNPs

The surface modification of AgNPs was performed using the one-phase ligand exchange method. For example, 5 mg of PAA was first dissolved into 20 mL of water. Then, 40 mL of AuNPs solution was concentrated down to about 0.2 mL. The concentrated AuNPs were slowly added into the PAA solution under vigorous stirring over a period of 24 h. PAA-grafted AuNPs were centrifuged three times to remove the free polymers. Similarly, citrate acid capped AgNPs were modified with the same procedures, using AgNPs instead of AuNPs.

pH-responsiveness of plasmonic NPs

Using PAA-grafted AuNPs as an example, 700 μL of PAA-grafted AuNP solution was transferred into a 1 mL plastic cuvette. Then, 5 μL of 0.05 M H_3PO_4 solution was continuously added to the same cuvette to drive the aggregation. The solution was analyzed using UV-vis spectroscopy to record the changes in the LSPR. To investigate the re-dispersion of PAA-grafted AuNPs, 0.05 M NaOH solution was added to the above solution until pH reached 12 and the color changed to red simultaneously. Meanwhile, the corresponding UV-vis spectra were recorded to monitor the change in the LSPR. By following similar steps, the reversibility was examined using H_3PO_4 and NaOH solutions at a much lower concentration. The aggregation of positively charged PAH-grafted AuNPs was monitored similarly by adding 5 μL of 0.05 M NaOH solution. The disassembly was examined with 0.1 M HCl solution. The process was analyzed similarly.

Surface-enhanced Raman spectra measurement

SERS measurements were carried out on a portable Raman spectrometer (QE Pro, Ocean Optics) with a 785 nm laser. To avoid any variation from different laser wavelengths, all experiments were tested under laser irradiation with the same wavelength. At the same time, the 785 nm portable Raman spectrometer has a spot size of *ca.* 1 cm; therefore, it provides an average SERS intensity with reliable readouts. For each Raman test, 130 μL of PAA-AgNP dispersion was injected into a 1.5 mL microcentrifuge tube. After adding the SERS probes to the

Open Access Article. Published on 22 2023. Downloaded on 2025/11/21 6:03:50.
This article is licensed under a Creative Commons Attribution 3.0 Unported Licence.

microcentrifuge tube, the solution was sonicated for 5 min. To induce the aggregation of NPs, *e.g.*, PAA-grafted AgNPs for SERS, 20 μL of 0.5 M H_3PO_4 was added to the same tube with manual shaking. The solution color changed from pale-yellow to black and the corresponding pH was tested. Then 100 μL of the mixture was transferred in a microcap. The solution was placed under laser irradiation for recording SERS four times for different testing sites. For each Raman measurement, the spectrum was collected for 5 scans. Similarly, after adding NaOH solution to tune the pH, the same testing steps were applied for SERS measurement under basic conditions.

Conflicts of interest

There are no conflicts to declare.

Acknowledgements

JH is grateful for the financial support from the National Science Foundation (CHE 2102245). The central instrumentation facilities at the Institute of Materials Science and Chemistry Department at UConn are acknowledged. The acquisition of the SAXS instrument was partially supported through an NSF grant (MRI-1228817).

References

1 J. Langer, D. Jimenez de Aberasturi, J. Aizpurua, R. A. Alvarez-Puebla, B. Auguié, J. J. Baumberg, G. C. Bazan, S. E. J. Bell, A. Boisen, A. G. Brolo, J. Choo, D. Cialla-May, V. Deckert, L. Fabris, K. Faulds, F. J. García de Abajo, R. Goodacre, D. Graham, A. J. Haes, C. L. Haynes, C. Huck, T. Itoh, M. Käll, J. Kneipp, N. A. Kotov, H. Kuang, E. C. Le Ru, H. K. Lee, J.-F. Li, X. Y. Ling, S. A. Maier, T. Mayerhöfer, M. Moskovits, K. Murakoshi, J.-M. Nam, S. Nie, Y. Ozaki, I. Pastoriza-Santos, J. Perez-Juste, J. Popp, A. Pucci, S. Reich, B. Ren, G. C. Schatz, T. Shegai, S. Schlücker, L.-L. Tay, K. G. Thomas, Z.-Q. Tian, R. P. Van Duyne, T. Vo-Dinh, Y. Wang, K. A. Willets, C. Xu, H. Xu, Y. Xu, Y. S. Yamamoto, B. Zhao and L. M. Liz-Marzán, Present and Future of Surface-Enhanced Raman Scattering, *ACS Nano*, 2020, **14**, 28–117.

2 L. J. Sherry, R. Jin, C. A. Mirkin, G. C. Schatz and R. P. Van Duyne, Localized Surface Plasmon Resonance Spectroscopy of Single Silver Triangular Nanoprisms, *Nano Lett.*, 2006, **6**, 2060–2065.

3 T. Itoh, M. Procházka, Z.-C. Dong, W. Ji, Y. S. Yamamoto, Y. Zhang and Y. Ozaki, Toward a New Era of Sers and Ters at the Nanometer Scale: From Fundamentals to Innovative Applications, *Chem. Rev.*, 2023, **123**, 1552–1634.

4 K. A. Willets and R. P. Van Duyne, Localized Surface Plasmon Resonance Spectroscopy and Sensing, *Annu. Rev. Phys. Chem.*, 2007, **58**, 267–297.

5 C. Zong, M. Xu, L.-J. Xu, T. Wei, X. Ma, X.-S. Zheng, R. Hu and B. Ren, Surface-Enhanced Raman Spectroscopy for Bioanalysis: Reliability and Challenges, *Chem. Rev.*, 2018, **118**, 4946–4980.

6 M. D. Porter, R. J. Lipert, L. M. Siperko, G. Wang and R. Narayanan, Sers as a Bioassay Platform: Fundamentals, Design, and Applications, *Chem. Soc. Rev.*, 2008, **37**, 1001–1011.

7 X. Li, T. Zhang, Z. Chen, J. Yu, A. Cao, D. Liu, W. Cai and Y. Li, Au Polyhedron Array with Tunable Crystal Facets by Pvp–Assisted Thermodynamic Control and Its Sharp Shape as Well as High–Energy Exposed Planes Co–Boosted Sers Activity, *Small*, 2022, **18**, 2105045.

8 D. Liu, L. Fang, F. Zhou, H. Li, T. Zhang, C. Li, W. Cai, Z. Deng, L. Li and Y. Li, Ultrasensitive and Stable Au Dimer–Based Colorimetric Sensors Using the Dynamically Tunable Gap–Dependent Plasmonic Coupling Optical Properties, *Adv. Funct. Mater.*, 2018, **28**, 1707392.

9 D. Men, F. Zhou, L. Hang, X. Li, G. Duan, W. Cai and Y. Li, A Functional Hydrogel Film Attached with a 2d Au Nanosphere Array and Its Ultrahigh Optical Diffraction Intensity as a Visualized Sensor, *J. Mater. Chem. C*, 2016, **4**, 2117–2122.

10 D. Men, D. Liu and Y. Li, Visualized Optical Sensors Based on Two/Three-Dimensional Photonic Crystals for Biochemicals, *Sci. Bull.*, 2016, **61**, 1358–1371.

11 S. Nie and S. R. Emory, Probing Single Molecules and Single Nanoparticles by Surface-Enhanced Raman Scattering, *science*, 1997, **275**, 1102–1106.

12 R. Chikkaraddy, B. De Nijs, F. Benz, S. J. Barrow, O. A. Scherman, E. Rosta, A. Demetriadou, P. Fox, O. Hess and J. J. Baumberg, Single-Molecule Strong Coupling at Room Temperature in Plasmonic Nanocavities, *Nature*, 2016, **535**, 127–130.

13 K. Saha, S. S. Agasti, C. Kim, X. Li and V. M. Rotello, Gold Nanoparticles in Chemical and Biological Sensing, *Chem. Rev.*, 2012, **112**, 2739–2779.

14 L. Velleman, L. Scarabelli, D. Sikdar, A. A. Kornyshev, L. M. Liz-Marzán and J. B. Edel, Monitoring Plasmon Coupling and Sers Enhancement through in Situ Nanoparticle Spacing Modulation, *Faraday Discuss.*, 2017, **205**, 67–83.

15 K. Chandra, K. S. B. Culver, S. E. Werner, R. C. Lee and T. W. Odom, Manipulating the Anisotropic Structure of Gold Nanostars Using Good's Buffers, *Chem. Mater.*, 2016, **28**, 6763–6769.

16 P. Zheng, M. Li, R. Jurevic, S. K. Cushing, Y. Liu and N. Wu, A Gold Nanohole Array Based Surface-Enhanced Raman Scattering Biosensor for Detection of Silver(I) and Mercury (Ii) in Human Saliva, *Nanoscale*, 2015, **7**, 11005–11012.

17 J. M. Romo-Herrera, R. A. Alvarez-Puebla and L. M. Liz-Marzán, Controlled Assembly of Plasmonic Colloidal Nanoparticle Clusters, *Colloidal Synth. Plasmonic Nanomet.*, 2020, 321–353.

18 G. Chen, Y. Wang, L. H. Tan, M. Yang, L. S. Tan, Y. Chen and H. Chen, High-Purity Separation of Gold Nanoparticle Dimers and Trimers, *J. Am. Chem. Soc.*, 2009, **131**, 4218–4219.

 This journal is © The Royal Society of Chemistry 2024

Open Access Article. Published on 22 2023. Downloaded on 2025/11/21 6:03:50.
This article is licensed under a Creative Commons Attribution 3.0 Unported Licence.

19 A. W. Wark, R. J. Stokes, S. B. Darby, W. E. Smith and D. Graham, Dynamic Imaging Analysis of Sers-Active Nanoparticle Clusters in Suspension, *J. Phys. Chem. C*, 2010, **114**, 18115–18120.
20 K. H. Su, Q. H. Wei, X. Zhang, J. J. Mock, D. R. Smith and S. Schultz, Interparticle Coupling Effects on Plasmon Resonances of Nanogold Particles, *Nano Lett.*, 2003, **3**, 1087–1090.
21 P. K. Jain, W. Huang and M. A. El-Sayed, On the Universal Scaling Behavior of the Distance Decay of Plasmon Coupling in Metal Nanoparticle Pairs: A Plasmon Ruler Equation, *Nano Lett.*, 2007, **7**, 2080–2088.
22 B. M. Reinhard, M. Siu, H. Agarwal, A. P. Alivisatos and J. Liphardt, Calibration of Dynamic Molecular Rulers Based on Plasmon Coupling between Gold Nanoparticles, *Nano Lett.*, 2005, **5**, 2246–2252.
23 A. J. Haes, S. Zou, G. C. Schatz and R. P. Van Duyne, Nanoscale Optical Biosensor: Short Range Distance Dependence of the Localized Surface Plasmon Resonance of Noble Metal Nanoparticles, *J. Phys. Chem. B*, 2004, **108**, 6961–6968.
24 W. Zhang, J.-B. You, J. Liu, X. Xiong, Z. Li, C. E. Png, L. Wu, C.-W. Qiu and Z.-K. Zhou, Steering Room-Temperature Plexcitonic Strong Coupling: A Diexcitonic Perspective, *Nano Lett.*, 2021, **21**, 8979–8986.
25 Y. Ofir, B. Samanta and V. M. Rotello, Polymer and Biopolymer Mediated Self-Assembly of Gold Nanoparticles, *Chem. Soc. Rev.*, 2008, **37**, 1814–1825.
26 C. Yi, Y. Yang, B. Liu, J. He and Z. Nie, Polymer-Guided Assembly of Inorganic Nanoparticles, *Chem. Soc. Rev.*, 2020, **49**, 465–508.
27 H. Duan, Y. Yang, Y. Zhang, C. Yi, Z. Nie and J. He, What Is Next in Polymer-Grafted Plasmonic Nanoparticles?, *Giant*, 2020, **4**, 100033.
28 H. Duan, Y. Lin and J. He, Metal Nanoparticles Grafted with Polymeric Ligands: Self-Assembly Guided by Polymers in Solution, in *Encyclopedia of Nanomaterials*, ed. Y. Yin, Y. Lu and Y. Xia, Elsevier, Oxford, 1st edn, 2023, pp. 390–406.
29 L. Cheng, A. Liu, S. Peng and H. Duan, Responsive Plasmonic Assemblies of Amphiphilic Nanocrystals at Oil–Water Interfaces, *ACS Nano*, 2010, **4**, 6098–6104.
30 H. Tao, E. Galati and E. Kumacheva, Temperature-Responsive Self-Assembly of Nanoparticles Grafted with Ucst Polymer Ligands, *Macromolecules*, 2018, **51**, 6021–6027.
31 M. Das, L. Mordoukhovski and E. Kumacheva, Sequestering Gold Nanorods by Polymer Microgels, *Adv. Mater.*, 2008, **20**, 2371–2375.
32 Y. Chen, Z. Wang, Y. He, Y. J. Yoon, J. Jung, G. Zhang and Z. Lin, Light-Enabled Reversible Self-Assembly and Tunable Optical Properties of Stable Hairy Nanoparticles, *Proc. Natl. Acad. Sci. U. S. A.*, 2018, **115**, E1391–E1400.
33 G.-H. Kim, M. Kim, J. K. Hyun and S.-J. Park, Directional Self-Assembly of Nanoparticles Coated with Thermoresponsive Block Copolymers and Charged Small Molecules, *ACS Macro Lett.*, 2023, **12**, 986–992.
34 C. Rossner, T. A. F. König and A. Fery. Hairy Plasmonic Nanoparticles, in *Hairy Nanoparticles*, 2023, pp. 351–374.
35 Z. Wei and J. He, Hairy Metal Nanoparticles for Catalysis: Polymer Ligand-Mediated Catalysis, in *Hairy Nanoparticles*, 2023, pp. 375–400.
36 P. Gu, J. Xu and J. Zhu, Self–Assembly of Polymer–Grafted Inorganic Nanoparticles into Three–Dimensional Superlattices, *Giant*, 2022, **12**, 100123.
37 Z. Nie, D. Fava, E. Kumacheva, S. Zou, G. C. Walker and M. Rubinstein, Self-Assembly of Metal–Polymer Analogues of Amphiphilic Triblock Copolymers, *Nat. Mater.*, 2007, **6**, 609–614.
38 J. He, Y. Liu, T. Babu, Z. Wei and Z. Nie, Self-Assembly of Inorganic Nanoparticle Vesicles and Tubules Driven by Tethered Linear Block Copolymers, *J. Am. Chem. Soc.*, 2012, **134**, 11342–11345.
39 C. Yi, H. Liu, S. Zhang, Y. Yang, Y. Zhang, Z. Lu, E. Kumacheva and Z. Nie, Self-Limiting Directional Nanoparticle Bonding Governed by Reaction Stoichiometry, *Science*, 2020, **369**, 1369–1374.
40 H. Duan, T. Malesky, J. Wang, C.-H. Liu, H. Tan, M.-P. Nieh, Y. Lin and J. He, Patchy Metal Nanoparticles with Polymers: Controllable Growth and Two-Way Self-Assembly, *Nanoscale*, 2022, **14**, 7364–7371.
41 J. He, X. Huang, Y.-C. Li, Y. Liu, T. Babu, M. A. Aronova, S. Wang, Z. Lu, X. Chen and Z. Nie, Self-Assembly of Amphiphilic Plasmonic Micelle-Like Nanoparticles in Selective Solvents, *J. Am. Chem. Soc.*, 2013, **135**, 7974–7984.
42 H. Duan, Z. Jia, M. Liaqat, M. D. Mellor, H. Tan, M.-P. Nieh, Y. Lin, S. Link, C. F. Landes and J. He, Site-Specific Chemistry on Gold Nanorods: Curvature-Guided Surface Dewetting and Supracolloidal Polymerization, *ACS Nano*, 2023, **17**, 12788–12797.
43 H. Tan, Y. Liu, J. Xie, Y. Gao, Y. Li, L. Ma, L. Zhang, T. Tang and J. Zhu, Light-Triggered Disassembly of Photo-Responsive Gold Nanovesicles for Controlled Drug Release, *Mater. Chem. Front.*, 2020, **4**, 2805–2811.
44 A. Lee, G. F. S. Andrade, A. Ahmed, M. L. Souza, N. Coombs, E. Tumarkin, K. Liu, R. Gordon, A. G. Brolo and E. Kumacheva, Probing Dynamic Generation of Hot-Spots in Self-Assembled Chains of Gold Nanorods by Surface-Enhanced Raman Scattering, *J. Am. Chem. Soc.*, 2011, **133**, 7563–7570.
45 J. Song, J. Zhou and H. Duan, Self-Assembled Plasmonic Vesicles of Sers-Encoded Amphiphilic Gold Nanoparticles for Cancer Cell Targeting and Traceable Intracellular Drug Delivery, *J. Am. Chem. Soc.*, 2012, **134**, 13458–13469.
46 L. Zhang, L. Dai, Y. Rong, Z. Liu, D. Tong, Y. Huang and T. Chen, Light-Triggered Reversible Self-Assembly of Gold Nanoparticle Oligomers for Tunable Sers, *Langmuir*, 2015, **31**, 1164–1171.
47 L. Liu, Z. Gao, B. Jiang, Y. Bai, W. Wang and Y. Yin, Reversible Assembly and Dynamic Plasmonic Tuning of Ag Nanoparticles Enabled by Limited Ligand Protection, *Nano Lett.*, 2018, **18**, 5312–5318.
48 T. Zhang, J. Ge, Y. Hu and Y. Yin, A General Approach for Transferring Hydrophobic Nanocrystals into Water, *Nano Lett.*, 2007, **7**, 3203–3207.

Open Access Article. Published on 22 2023. Downloaded on 2025/11/21 6:03:50.
This article is licensed under a Creative Commons Attribution 3.0 Unported Licence.

49 J. Newman and G. Blanchard, Formation and Encapsulation of Gold Nanoparticles Using a Polymeric Amine Reducing Agent, *J. Nanopart. Res.*, 2007, **9**, 861–868.
50 Z. Wei, M. Kayceety, A. Price, K. Wei, Q. Luo, S. Thanneeru, S. Sun and J. He, Polymer N-Heterocyclic Carbene (Nhc) Ligands for Silver Nanoparticles, *ACS Appl. Mater. Interfaces*, 2022, **14**, 55227–55237.
51 T. Swift, L. Swanson, M. Geoghegan and S. Rimmer, The Ph-Responsive Behaviour of Poly (Acrylic Acid) in Aqueous Solution Is Dependent on Molar Mass, *Soft Matter*, 2016, **12**, 2542–2549.
52 W. Li, I. Kanyo, C.-H. Kuo, S. Thanneeru and J. He, Ph-Programmable Self-Assembly of Plasmonic Nanoparticles: Hydrophobic Interaction Versus Electrostatic Repulsion, *Nanoscale*, 2015, **7**, 956–964.
53 Y. Kang and T. A. Taton, Core/Shell Gold Nanoparticles by Self-Assembly and Crosslinking of Micellar, Block-Copolymer Shells, *Angew. Chem., Int. Ed.*, 2005, **44**, 409–412.
54 S. Chakraborty and C. L. Kitchens, Modifying Ligand Chemistry to Enhance Reusability of Ph-Responsive Colloidal Gold Nanoparticle Catalyst, *J. Phys. Chem. C*, 2019, **123**, 26450–26459.
55 S. M. Ansar, B. Fellows, P. Mispireta, O. T. Mefford and C. L. Kitchens, Ph Triggered Recovery and Reuse of Thiolated Poly(Acrylic Acid) Functionalized Gold Nanoparticles with Applications in Colloidal Catalysis, *Langmuir*, 2017, **33**, 7642–7648.
56 C.-A. Fustin, C. Colard, M. Filali, P. Guillet, A.-S. Duwez, M. A. R. Meier, U. S. Schubert and J.-F. Gohy, Tuning the Hydrophilicity of Gold Nanoparticles Templated in Star Block Copolymers, *Langmuir*, 2006, **22**, 6690–6695.
57 K. Kim, J.-Y. Choi and K. S. Shin, Surface-Enhanced Raman Scattering of 4-Nitrobenzenethiol and 4-Aminobenzenethiol on Silver in Icy Environments at Liquid Nitrogen Temperature, *J. Phys. Chem. C*, 2014, **118**, 11397–11403.
58 K. Zhang, G. Li and Y. Hu, In Situ Loading of Well-Dispersed Silver Nanoparticles on Nanocrystalline Magnesium Oxide for Real-Time Monitoring of Catalytic Reactions by Surface Enhanced Raman Spectroscopy, *Nanoscale*, 2015, **7**, 16952–16959.
59 Y. Tzeng and B.-Y. Lin, Silver Sers Adenine Sensors with a Very Low Detection Limit, *Biosensors*, 2020, **10**, 53.
60 F.-H. Cho, S.-C. Kuo and Y.-H. Lai, Surface-Plasmon-Induced Azo Coupling Reaction between Nitro Compounds on Dendritic Silver Monitored by Surface-Enhanced Raman Spectroscopy, *RSC Adv.*, 2017, **7**, 10259–10265.
61 M. Poonia, T. Küster and G. D. Bothun, Organic Anion Detection with Functionalized Sers Substrates Via Coupled Electrokinetic Preconcentration, Analyte Capture, and Charge Transfer, *ACS Appl. Mater. Interfaces*, 2022, **14**, 23964–23972.
62 H. He, P. Li, X. Tang, D. Lin, A. Xie, Y. Shen and L. Yang, Developing Cysteamine-Modified Sers Substrate for Detection of Acidic Pigment with Weak Surface Affinity, *Spectrochim. Acta, Part A*, 2019, **212**, 293–299.
63 H. Li, H. Xia, W. Ding, Y. Li, Q. Shi, D. Wang and X. Tao, Synthesis of Monodisperse, Quasi-Spherical Silver Nanoparticles with Sizes Defined by the Nature of Silver Precursors, *Langmuir*, 2014, **30**, 2498–2504.

This journal is © The Royal Society of Chemistry 2024